HIGH-SPEED, LOW-POWER, LOW-PROFILE DESIGN FIBER-OPTIC COMMUNICATION SYSTEM FOR CUBESAT

A Thesis
Presented to
The Academic Faculty

By

Kohei Kotani

In Partial Fulfillment
of the Requirements for the Degree
Masters in the
School of Aerospace Engineering
Department of Aerospace Engineering

Georgia Institute of Technology

August 2022

HIGH-SPEED, LOW-POWER, LOW-PROFILE DESIGN FIBER-OPTIC COMMUNICATION SYSTEM FOR CUBESAT

Thesis committee:

Dr. Brian Gunter
Aerospace Engineering
Georgia Institute of Technology

Dr. Christopher Carr
Aerospace Engineering
Georgia Institute of Technology

Dr. Glenn Lightsey
Aerospace Engineering
Georgia Institute of Technology

Date approved: May 12, 2022

TABLE OF CONTENTS

LIST OF TABLES

LIST OF FIGURES

LIST OF ACRONYMS

ADC analog-to-digital converter

DMA direct memory access

EMI electromagnetic interference

FFC flat flexible cable

FIFO first-in first-out

FPGA field programmable gate array

GPIO general-purpose input/output

HDL hardware description language

IP intellectual property

LEO low-earth orbit

LET linear energy transfer

LUT look-up table

LVDS low-voltage differential signal

MCU micro-controller unit

MGT multi-gigabit transceiver

MSB most-significant bit

PCB printed circuit board

RAM random access memory

RF radio frequency

RPiCM4 Raspberry Pi Compute Module 4

RTL registerr-transfer level

RX receiver

SAR synthetic aperture radar

SEE single event effects

SET single event transient

TX transceiver

SUMMARY

Today, the demand for big data, such as high-resolution images, has been rapidly increasing in space missions. However, the means to achieve multi-Gbps transmission is limited to ethernet, coax, or flat flexible cable (FFC) in CubeSat design. This research describes the development of a lightweight and low-power consumption high-speed communication system suitable for small satellites. A high volume of data from two high-resolution cameras is transmitted to a Raspberry Pi Compute Module 4 running Linux using a fiber-optic link as an interconnect, and the dual images are displayed on a monitor. The FPGA with a high-speed transceiver is extensively used to achieve high-speed communication. It is also verified that the fiber-optic module operates at up to 6.25 Gbps with a power consumption of 90 mW.

This research includes the hardware and software development details. All the materials, including the schematics, printed circuit board (PCB) design, and programming codes, can be found in the Github repository(https://github.com/kotaniko/dual-imaging).

Furthermore, this thesis includes the discussion of fiber-optic module usage in the space environment and comparing fiber-optic with ethernet, coax, and FFC, along with the selection guides CubeSat developers can refer to.

The final deliverable of this research is the high-speed fiber-optic interconnection designed to fit into a CubeSat platform, demonstrating the dual-image display from two HD cameras. The prototype can be extended to implement high-volume data applications such as stereo imaging for proximity operations, free-space inter-satellite links, and high-speed intra-satellite communications for CubeSat platforms.

CHAPTER 1
INTRODUCTION AND BACKGROUND

1.1 Introduction

First used in a space mission in 1992, fiber-optic communications have been utilized in orbit to achieve high-speed interconnections[1]. Since then, the demand for big data, such as high-resolution images and synthetic aperture radars, has rapidly increased in space missions. Fiber-optic interconnections have advantages such as low power consumption, low signal attenuation, improved electrical isolation, high electromagnetic interference (EMI) tolerance, and a lightweight and low-profile design with flexible cables, which are desirable characteristics for CubeSat design with strict constraints on mass, volume, and power budget. However, the means to achieve multi-Gbps transmission has previously been limited to ethernet, coax, or flat flexible cable (FFC) in CubeSat designs. Furthermore, small satellites, including CubeSats, are adopting higher carrier frequencies for radio frequency (RF) communications to achieve higher data rates in recent years because of the increased amount of sensor data. Future CubeSat designs need higher data-rate interconnections at a rate of multi-Gbps to accommodate the increasing demand for the high volume of data, such as high-resolution cameras. Now that several commercial off-the-shelf fiber-optic modules are available, the feasibility of fiber-optic interconnections in CubeSat platforms should be tested. Hence, this research focused on implementing a high-speed interconnection for CubeSat platforms with the BF4M fiber-optic module. Additionally, my interests lie in hardware and low-level software development. Hence, it is suitable for my master thesis to develop a prototype for a high-speed fiber-optic communication system for CubeSat to promote technological advancement and satisfy my curiosity.

This research demonstrates the hypothesis that using a lightweight, low-profile, and

low-power fiber-optic module with a flexible fiber cable for subsystem interconnections allows for flexible CubeSat design and enables the high-speed data transmission of up to 6.25 Gbps from payload sensors. Since ready-to-use fiber-optic interconnection systems are not commercially available, interconnection subsystems must be designed for each application using fiber-optic modules and processors with high-speed transceivers. The thesis also analyzes and compares the fiber-optic module with ethernet, coax, and FFC, current solutions to high-speed communication in CubeSat platforms.

This research focuses on the technical development of fiber-optic communication systems using an Artix-7 FPGA, Raspberry Pi Compute Module 4, the Pcam 5C camera modules, and the BF4M fiber-optic module. This research does not evaluate the environmental testing on the BF4M fiber-optic module in the space environment, such as thermal cycling and vibration tests. However, a final prototype design could be used for vibration tests in the future, and reference work presented in Section 3.1 shows it is likely that commercial off-the-shelf fiber-optic transceivers can tolerate the space environment. In addition to verifying this hypothesis, hardware and software development details are documented and uploaded to a GitHub repository(https://github.com/kotaniko/dual-imaging) for future CubeSat developers.

The development of a dual imaging display to prove the concept of fiber-optic usage in a CubeSat platform is discussed in Chapter 2. In Section 3.1, the preliminary results on the operation of fiber-optic modules in the space environment are presented. Section 3.2 introduces space-grade fiber-optic modules already commercially available. Section 3.3 compares the fiber-optic module with the traditional data transfer methods of ethernet, coax, and FFC from multiple aspects, including the maximum bandwidth, cable flexibility, power consumption, transmission length, cable weight, and connector size. Some of the potential application examples utilizing fiber-optic communication are elaborated in Section 4.1. Although this thesis mainly discusses the excellence of a fiber-optic module, it is not always the best solution to many missions. Reference guides are presented in Sec-

tion 4.2 to help CubeSat designers to decide when to select a fiber-optic module. Finally, Chapter 5 concludes the findings of this research.

CHAPTER 2
PROOF OF CONCEPT PROTOTYPING

By implementing this dual image display as one example of possible applications, the effectiveness of the high-speed fiber-optic communication system is established, and the hypothesis of this research that using a fiber optic link enables CubeSat to handle high-speed data transmissions of 1.0 Gbps or more from payload sensors can be verified. Furthermore, this success demonstrates that Cubesat developers with limitations in power consumption, space, and weights have a solution for multi-gigabit transfers with a more flexible design.

2.1 Dual-Imaging Display

To demonstrate the ability of the fiber-optic communication system, the dual-image display is developed in this research. Two HD-resolution cameras yield raw images at 30 frames-per-second each producing $1920\,[\text{width}] \times 1080\,[\text{height}] \times 16\,[\text{bits/frame}] \times 30\,[\text{fps}] \times 2 = 1.99$ Gbps of data in total. The produced data is finally transferred to a single board computer via a fiber-optic cable and stored in its random access memory (RAM) at the reduced rate of 15 fps. The data stored in the RAM is playable on a monitor connected to the single board computer.

Here, the two HD cameras are analogous to any sensor that generates the data over 1.0 Gbps. Thus, the two HD cameras can be substituted with any high data-rate sensor to achieve different applications. The details of the hardware and software setup of this demonstration are discussed in Section 2.3 and Section 2.5.

2.2 Proposed Objectives and Final Deliverables

Below is a list of milestones achieved regarding the hardware and software development for this study.

1. Hardware Development
    1. Schematic Design
    2. PCB Design
    3. PCB Manufacturing
    4. Soldering
    5. Continuity Check
2. Software Development
    1. FPGA JTAG Programming Check
    2. Raspberry Pi CM4 Setup
    3. BF4M Bandwidth Check and Power Consumption Measurement
    4. Camera Image Acquisition
    5. RX FPGA board and Raspberry Pi CM4 I/O via PCIe
    6. Dual-Image Display on RPiCM4

In this research, the minimum success criteria was to achieve the data transfer from the transceiver (TX) board to the receiver (RX) board at 1.0 Gbps or higher. Section 2.4 discusses how the bandwidth of the BF4M module is measured and the results. This validation of the bandwidth was completed at the FPGA-level with VHDL programming; thus, Raspberry Pi Compute Module 4 (RPiCM4) will not be needed to show the minimum success.

One key research objective was to produce high-resolution dual images on the RPiCM4. This prototype demonstrates transferring two high-resolution raw images at 15 fps. The

data-rate required for this demonstration is 1920×1080 [pixels/frame] $\times$ 16 [bits/pixel] $\times$ 15 [fps] $\times$ 2 $\approx$ 1.00 Gbps, and the details of the dual image display are discussed in Section 2.5.

Github repository (https://github.com/kotaniko/dual-imaging.git) is created as well. This repository can reference future CubeSat designers aiming to utilize the fiber optic module with FPGA. The repository has detailed documentation regarding the prototype, and schematics, PCB design, C code, and scripts used in the Raspberry Pi Compute Module 4 are available.

2.3 Hardware System Architecture

2.3.1 Hardware Selection

The following hardware was selected amid the semiconductor shortage in 2021.

- Hirose BF4M fiber-optic module [Figure 2.1]
  - Fiber optic cable with optical-electrical converters

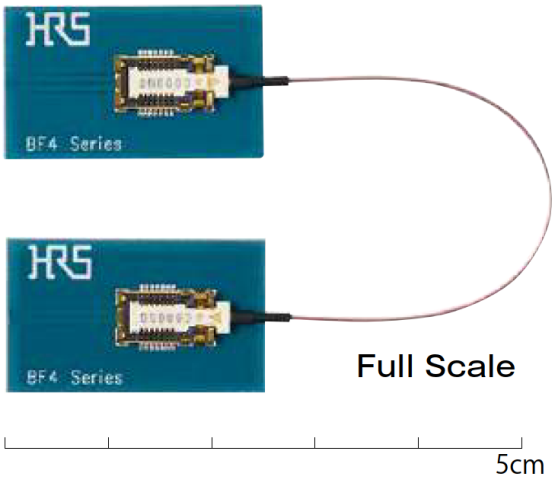

Figure 2.1: Image of BF4M

- Digilent Pcam 5C [Figure 2.2]

- Capable of outputting 1920x1080 resolution image at 30 fps in the Bayer format with the MIPI CSI interface

Figure 2.2: Image of Pcam5C

- Trenz TE0714 Rev. 3 [Figure 2.3]
  - field programmable gate array (FPGA) board embedding XC7A50T-2CSG325I with a multi-gigabit transceiver (MGT) capable of up to 6.25 Gbps data transfer

Figure 2.3: Image of TE0714

- Raspberry Pi Compute Module 4 [Figure 2.4]
  - Single board computer embedding quad-core Cortex-A72 64-bit SoC and 4 GB RAM

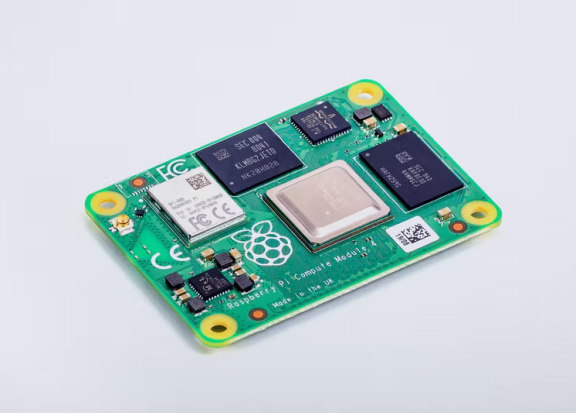

Figure 2.4: Image of Raspberry Pi Compute Module 4

Among the number of fiber optic cables, the BF4M was selected as it was readily available from major vendors at a reasonable price of $100/m. The BF4M is also a small factor, as shown in Figure 2.1. The BF4M's cable weight and its connector size are discussed in Subsection 3.3.5 and Subsection 3.3.6, respectively.

The Pcam 5C was selected as Digilent offers the demo project using the Pcam5C on a Zynq-7000 ARM/FPGA Soc development board. Using this demo project as a reference enabled a fast prototype development.

The TE0714 integrates an Artix-7 50T with a MGT capable of data transfer up to 6.25 Gbps. The TE0714 development board was chosen because of a reasonable price of approximately $150 per board and can maximize the bandwidth of the BF4M.

The options of development boards were limited amid the semiconductor shortage in 2021. If available, a development board hosting a SoC FPGA with a MGT such as the Zynq-7015 series should be selected. SoC FPGA eliminates the need for high-speed transmission between the TE0714 and the Raspberry Pi CM4, facilitates the development of the system, and possibly offers better performance.

Table 2.1 summaries the price of each hardware component as of 2021.

Table 2.1: BOM list

Component Name	Price
BF4M	$100
TE0714	$150
JTAG-HS3	$60
Raspberry Pi Compute Module 4	$60
Pcam 5C	$90
Passive Components, Connectors, Power ICs	$45
PCB	$102
Total	$607

2.3.2 System Diagram

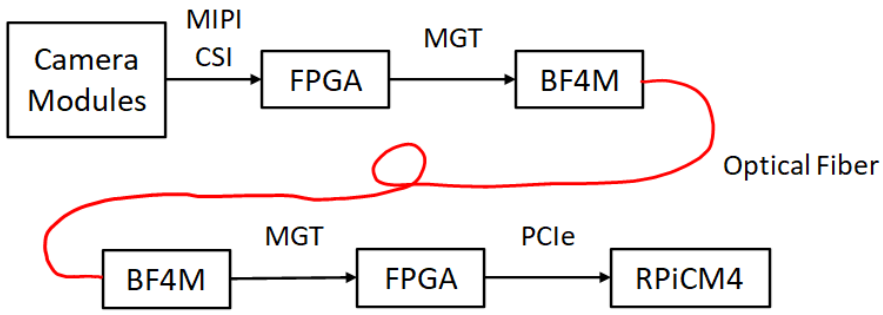

Figure 2.5: System overview of the prototype

Figure 2.5 shows the overview of this prototype. The two Pcam 5C cameras produce images of 1920×1080 pixels at 30 fps in the Bayer format with the MIPI CSI standard. The TX FPGA board converts the Bayer format to the BGR565 format and transmits the data to the RX FPGA board via the BF4M fiber-optic module. In the RX FPGA board, the data rate of the images are reduced from 30 fps to 15 fps due to the limitation of the Raspberry Pi CM4. The data stream is then transmitted to the Raspberry Pi CM4 via PCIe. Thus, the Raspberry Pi CM4 receives and stores the data at a rate of $1920\,[\text{width}] \times 1080\,[\text{height}] \times 16\,[\text{bits/frame}] \times 15\,[\text{fps}] \times 2 \approx 1.00$ Gbps.

2.3.3 PCB Design

Two PCBs are designed for the TX and RX sides connected by the BF4M fiber-optic cable using KiCAD 6.0 and fabricated by OSHPark. The BF4M module transfers the data from the TX board to the RX board with a fiber-optic cable. The TX board hosts one TE0714, and the RX board hosts one TE0714 and Raspberry Pi CM4 connected via PCIe.

The PCB is designed as a two-layer to minimize the system's fabrication cost and complexity. Due to the physical limitation of the two-layer PCB, the 100 Ω differential impedance matching for the BF4M differential signaling traces and 90 Ω differential impedance matching for the PCIe traces could not be satisfied but attempted as close as possible. Four-layer PCB can reduce the isolation height to achieve the 100 Ω and 90 Ω differential impedance matching.

Additionally, the differential pairs such as MIPI CSI data and clock lanes, PCIe lanes, and the BF4M data lanes are length matched within 0.1 mm to satisfy the required signal integrity. Figure 2.6 shows the length matching for the MIPI CSI differential signaling traces.

The dimensions and fabrication costs of the TX and RX PCBs are shown in Table 2.2.

Table 2.2: PCB dimension and fabrication price by OSHPark

Board	Dimension(mm)	Price
TX	70x63	$34
RX	109x81	$68

2.4 Methods of Validation and Results

The hardware architecture is explained in the previous section. This section discusses the validation of the BF4M fiber-optic module and the results.

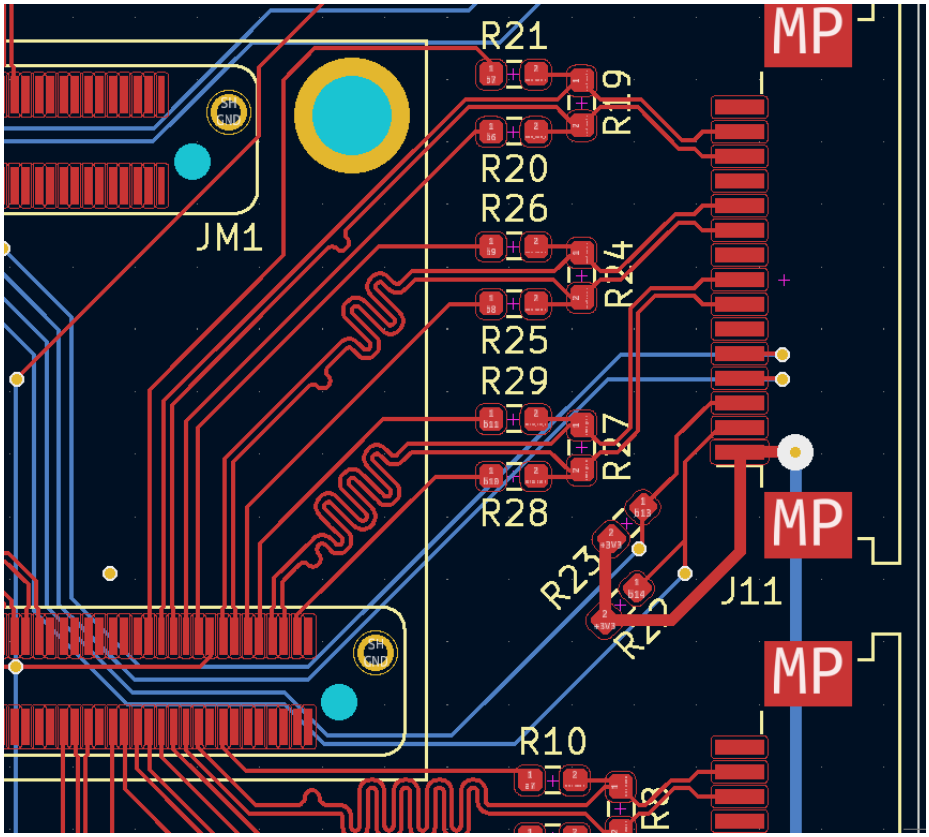

Figure 2.6: Image of PCB design

2.4.1 BF4M Bandwidth

The following scheme shown in Figure 2.7 is set up to measure the throughput of the BF4M module. Only FPGAs in the transceiver and receiver sides and the BF4M module are activated to simplify the system.

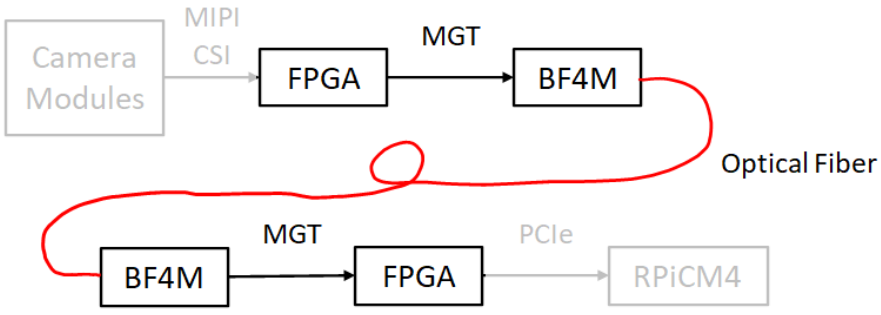

Figure 2.7: System overview of the validation

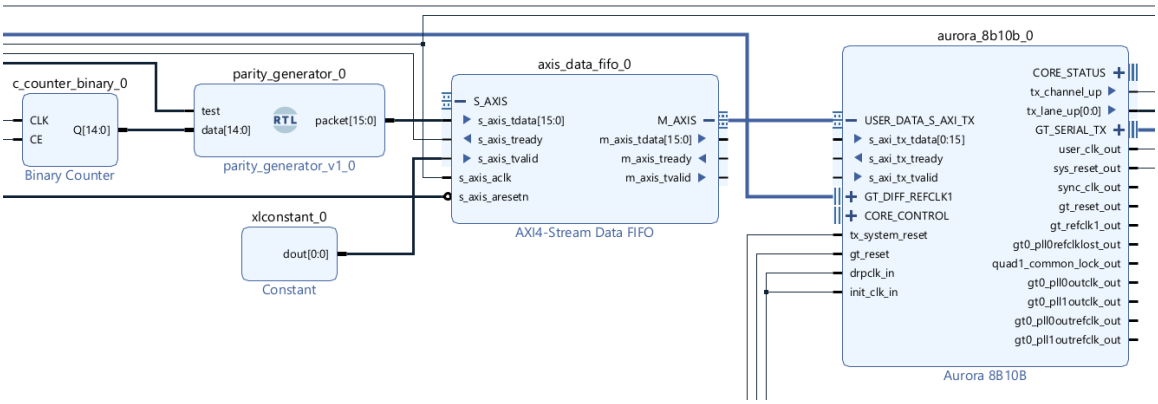

Figure 2.8: Block diagram of TX validation

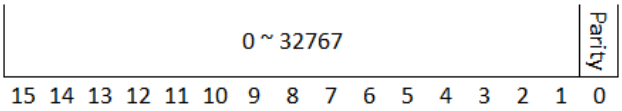

Figure 2.9: Packet structure used for bandwidth validation

Figure 2.8 shows the block diagram of the TX board. The Binary Counter core outputs the sequential counter value from 0 to 32767. The parity bit is generated using the counter value from the Binary Counter core in the user-made Parity Generator registerr-transfer level (RTL). The packet is then routed to the Aurora8B10B core, which transfers data to the BF4M module. Overall, the TX FPGA continuously sends the 16 bits of data consisting of the 15-bit number in most-significant bit (MSB) and the parity bit in Bit 0 as shown in Figure 2.9.

Figure 2.10 shows the block diagram of the RX board. The RX FPGA computes the parity of 15 significant bits of the received packet and compares the calculated parity with the parity bit in Bit 0 to determine the validity of the received packet. The RX FPGA flips the output level of one of the general-purpose input/output (GPIO) pins when the 15-bit number in the packet corresponds to 0x5555. Thus, the time it takes to flip the I/O pin is the time the BF4M takes to transfer 16×32767 bits. The bandwidth is computed by measuring the time of flipping the status of the GPIO pin with a logic analyzer sampling at 200 MHz as shown in Figure 2.11.

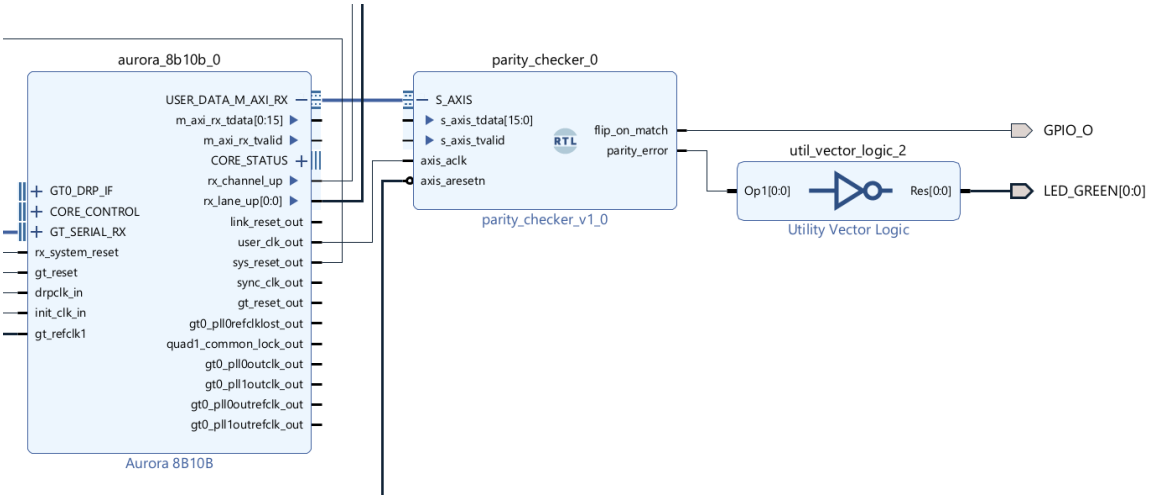

Figure 2.10: Block diagram of RX validation

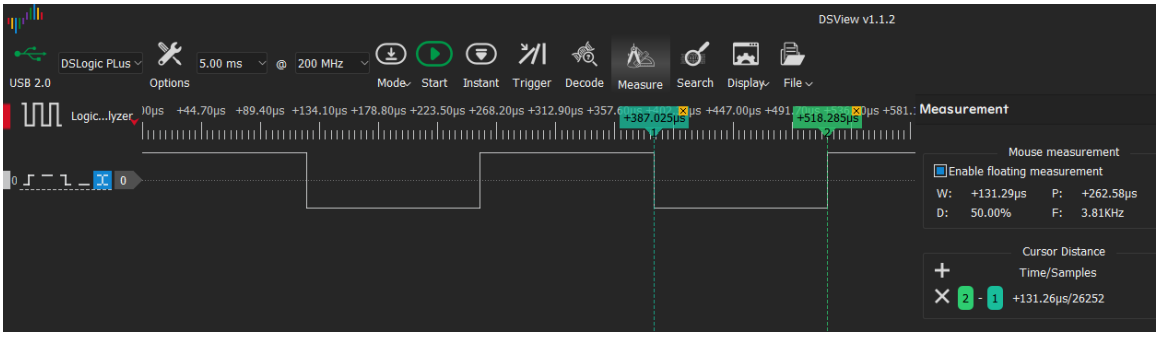

Figure 2.11: Time measurement with a logic analyzer at 5.0 Gbps

Table 2.3 summarizes the measured time, computed bandwidth, and parity match. The BF4M module operates at the expected bandwidth without error, from 2.0 Gbps to 6.25 Gbps.

Table 2.3: Measured bandwidth and parity results operating from 2.0 Gbps to 6.25 Gbps

Raw Bit BW	Effective BW	Time	Measured BW	Parity
2.0 Gbps	1.6 Gbps	328 us	1.60 Gbps	Error-free
2.5 Gbps	2.0 Gbps	263 us	1.99 Gbps	Error-free
3.125 Gbps	2.5 Gbps	210 us	2.50 Gbps	Error-free
4.0 Gbps	3.2 Gbps	164 us	3.20 Gbps	Error-free
5.0 Gbps	4.0 Gbps	131 us	4.00 Gbps	Error-free
6.25 Gbps	5.0 Gbps	105 us	4.99 Gbps	Error-free

It is noted that the effective bandwidth is 80 % of the configured bandwidth since the 8 bits of data are encoded to 10 bits for the clock recovery.

2.4.2 Power Consumption Measurement

The power consumption of the BF4M, TX board, and RX board operating from 2.0 Gbps to 6.25 Gbps is measured with a current sensor and summarized in Table 2.4.

Table 2.4: Power consumption of BF4M operating from 2.0 Gbps to 6.25 Gbps

Raw Bit BW	BF4M TX	BF4M RX	FPGA TX	FPGA RX
2.0 Gbps	22.4 mW	57.4 mW	603 mW	582 mW
2.5 Gbps	22.4 mW	57.4 mW	622 mW	599 mW
3.125 Gbps	22.4 mW	60.2 mW	644 mW	624 mW
4.0 Gbps	22.4 mW	60.2 mW	636 mW	610 mW
5.0 Gbps	22.4 mW	61.6 mW	661 mW	633 mW
6.25 Gbps	22.4 mW	64.4 mW	693 mW	661 mW

At any bandwidth, the BF4M module consumes less than 90 mW in total. Additionally, the power consumption of the TX and RX FPGA shown in Table 2.4 includes the power required for proper operation of FPGAs and other miscellaneous functionalities such as LED indicators.

2.5 Software System Architecture

The firmware for the FPGA boards is developed with a Xilinx Vivado 2021.2. The following sections discuss the software design of TX and RX FPGA.

2.5.1 TX FPGA board

Figure 2.12 shows the first part of the block diagram of the TX FPGA board.

MIPI CSI RX subsystem IP core is provided by Xilinx and establishes the connection between the FPGA and Pcam 5C with the MIPI CSI standard. The MIPI CSI standard is a licensed standard; thus, it is necessary to use the IP core to decode the MIPI CSI standard to extract the image data.

The output of the MIPI CSI RX subsystem is in the 10-bit Bayer format, which can not directly be used to display on the Raspberry Pi CM4. The Sensor Demosaic IP computes

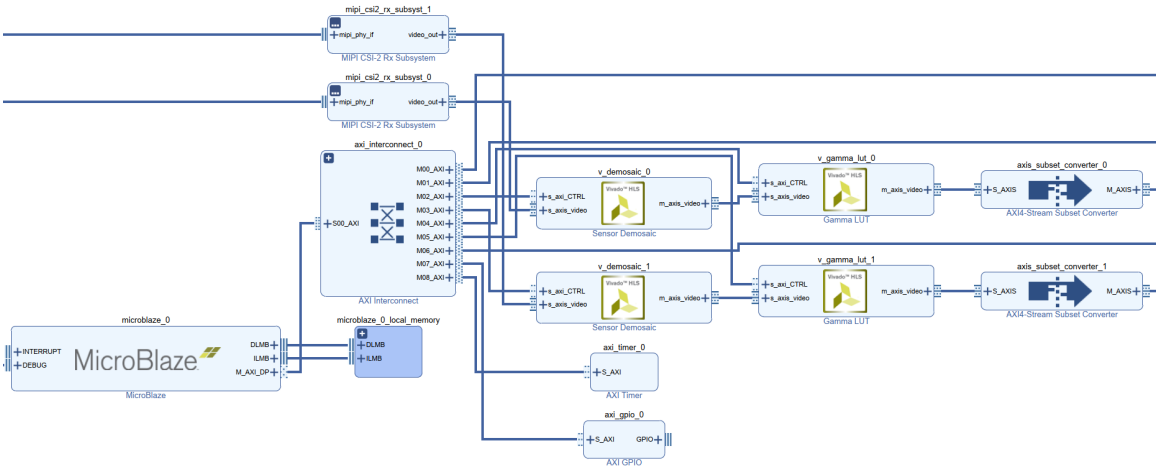

Figure 2.12: First part of the block diagram of the TX FPGA board

the RGB values of every pixel from the provided 10-bit Bayer format.

The Gamma look-up table (LUT) intellectual property (IP) core calibrates the brightness of images to compensate for the camera lens characteristics by applying a gamma function.

The outputs of the Gamma LUT IP consist of the 30-bit RGB values, so the width of the red, green, and blue components must be reduced to 5-bit, 6-bit, and 5-bit, respectively. The order of the color component is also reordered to BGR to match the format that ffplay can play on the Raspberry Pi CM4. AXI4-Stream Subset Converter core handles the width reduction and bits reordering.

The MicroBlaze core is a soft CPU used to control the GPIO, the Pcam 5C registers with I2C, and the Sensor Demosaic and Gamma LUT cores with the AXI-MemoryMapped interface.

Figure 2.14 shows the AXI-Stream interface of the MIPI CSI RX subsystem and Aurora8B10B core. The MIPI CSI RX subsystem IP core uses the tuser port in the AXI Stream interface to indicate the start of the frame in the MIPI CSI RX subsystem core. However, the Aurora8B10B core does not support the tuser port. Thus, another technique must be employed. Stream_mod, the user-made RTL, modifies the packet to a reserved value when

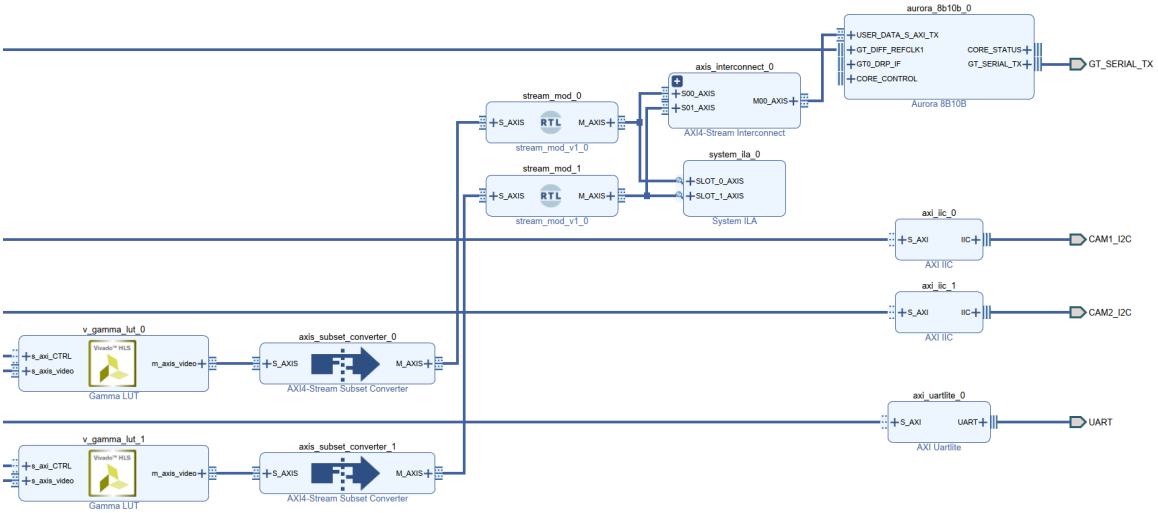

Figure 2.13: Second part of the block diagram of the TX FPGA board

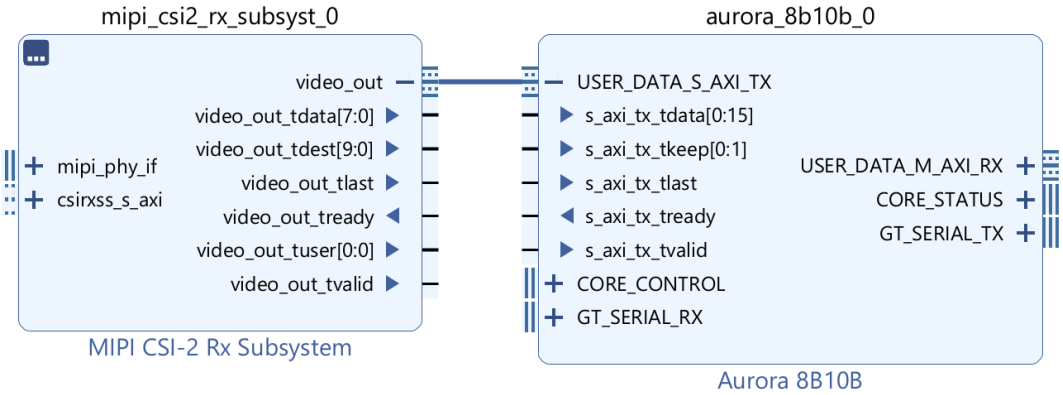

Figure 2.14: AXI-Stream ports of MIPI CSI RX subsystem and Aurora8B10B core

detecting the tuser port high. The stream_mod RTL also changes bit 5 of the data stream to 0 if the stream is coming from the first camera and 1 if the second camera. By modifying the data stream in such ways, the RX FPGA can detect the start of the frame and which camera module each packet belongs to.

Since the Aurora8B10B IP core takes 16-bits of data, and the data stream is also in 16-bits, the AXI4-Stream Interconnect IP core routes the two input streams to one output stream with a round-robin strategy.

2.5.2 RX FPGA board

Figure 2.15 is the block diagram of the RX FPGA board.

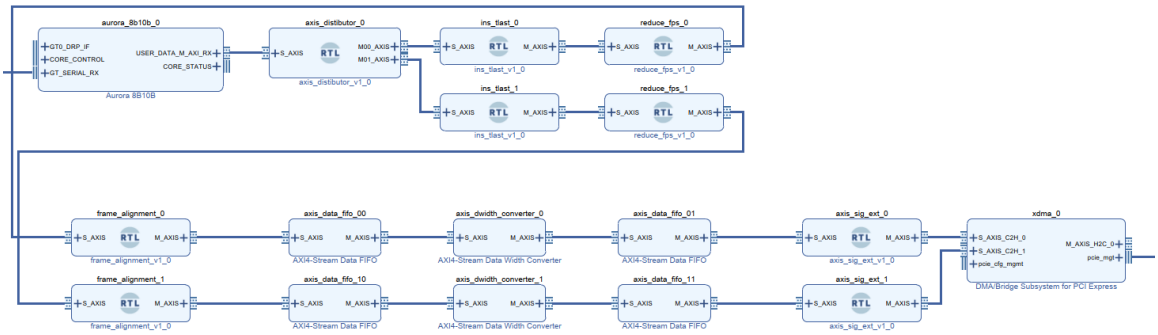

Figure 2.15: Block diagram of the RX FPGA board

The Aurora 8B10B IP core outputs the 16-bit width data from the BF4M. The 16-bit data stream with an identifier added at the stream_mod RTL in the TX FPGA is distributed to two 16-bit data streams.

The tlast bit in the AXI-Stream interface is added to the pixel corresponding to the last packet of the image frame at the user-made ins_tlast RTL. The data stream of images is reduced from 30 fps to 15 fps so that the Raspberry Pi CM4 can play them without dropping a frame. The data stream contains the reserved value for the first pixel as explained in Subsection 2.5.1. The frame_alignment RTL aligns the start of the frame by checking every value of the data stream and discards data before finding the first pixel of the frame. This alignment procedure ensures that the Raspberry Pi CM4 receives the first pixel when the PCIe transaction is requested.

Then, the data width is converted from 16-bit to 64-bit to be compatible with the data width of the DMA/Bridge Subsystem for the PCI Express IP core. The first-in first-out (FIFO) is inserted into the data stream to allow some buffering. The two data streams are connected to the two dedicated ports of the DMA/Bridge Subsystem for PCI Express IP core enabling the Raspberry Pi CM4 to choose which data stream to receive.

2.5.3 Raspberry Pi CM4 board

The 64-bit Raspberry OS is installed to enable the RAM usage over 4 GB and for the best compatibility with the Raspberry Pi CM4, as the OS is designed specifically for it. The XDMA driver is downloaded from the Xilinx Github repository, compiled, and installed to communicate the DMA/Bridge Subsystem for PCI Express IP core on the RX FPGA. The following commands copy the data from the PCIe device into the RAM (dd) and play the stored data on display (ffplay).

```
dd if=/dev/xdma0_c2h_0 ibs=1920x1080x2 count=90 of=/tmp/ram/out1 obs=32k
& dd if=/dev/xdma0_c2h_1 ibs=1920x1080x2 count=90 of=/tmp/ram/out2 obs=32k
```

This dd command transfers 90 frames from a channel of the PCIe core to a ramdisk. xdma0_c2h_0 is a channel connected to the data stream from camera 1, and xdma0_c2h_1 is from camera 2. Specifying the input block size of $1920 \times 1080 \times 2$, which is the size of one frame, showed the best performance.

```
ffplay -f rawvideo -pixel_format bgr565le -video_size 1920x1080 -framerate
15 /tmp/ram/out1
```

This ffplay command plays the raw video data from the specified path at the framerate of 15. Since the stored data does not come with a header, the user must specify the data structure, bgr565le, and the video size of 1920x1080.

2.5.4 Raspberry Pi CM4 Receiver Data-rate Limitation

It is found that the Raspberry Pi CM4 can handle the data stream from PCIe to /dev/null at 30 fps, but transferring the data to RAM at any rate over 15 fps results in the loss of data. Although the causes of reduced fps in the Raspberry Pi CM4 are not identified nor addressed in this research, the potential causes include the limited bandwidth from PCIe to RAM on the Raspberry Pi CM4, PCIe and other interrupts generated during the process, and OS system call overhead. This limitation is demonstrated in Section 2.7.

2.6 Images of Prototype

Figure 2.16 and Figure 2.17 show the prototype board from side and front.

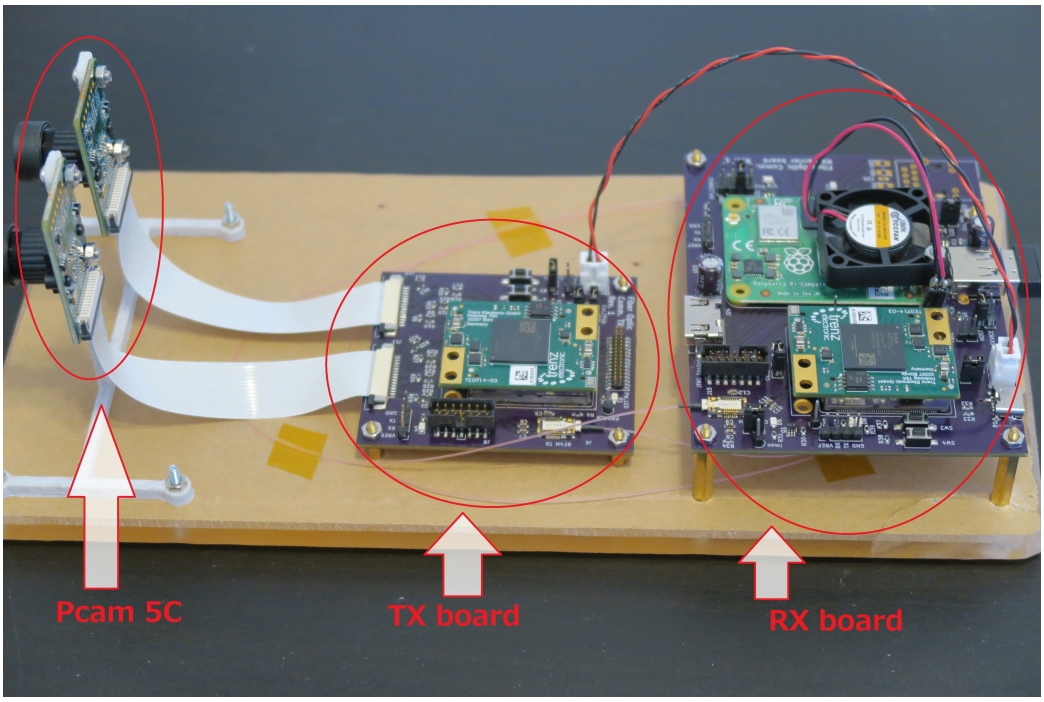

Figure 2.16: Side view of the prototype

Figure 2.18 shows the TX board. The board has the TE0714 FPGA board and the BF4M module.

Figure 2.19 shows the RX board. The board has the TE0714 FPGA, Raspberry Pi CM4, and BF4M modules.

2.7 Dual Image Display Demonstration

The video demonstrating the dual-image display on the Raspberry Pi CM4 is available at the Github repository. The video demonstrates displaying the images from the two camera modules at 15 fps. The throughput of this stream is $1920\,[\text{width}] \times 1080\,[\text{height}] \times 16\,[\text{bits/frame}] \times 15\,[\text{fps}] \times 2 \approx 1.00$ Gbps. Considering the TCP/IP overhead of ethernet, this outperforms the ethernet bandwidth. Though the Raspberry Pi CM4 was capable of

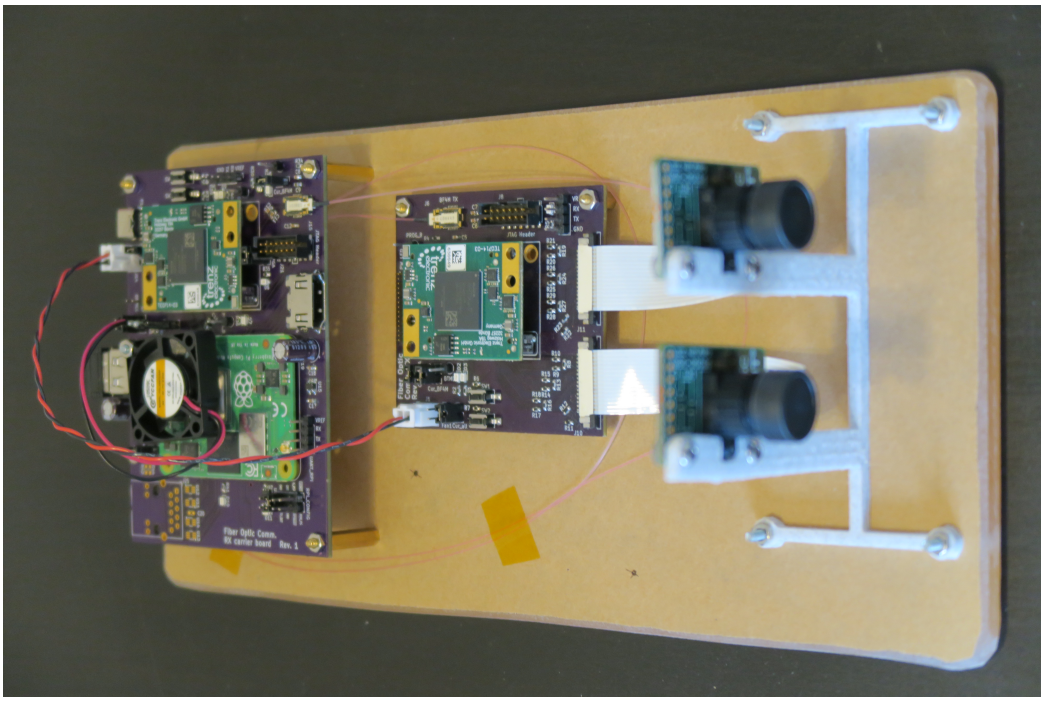

Figure 2.17: Front view of the prototype

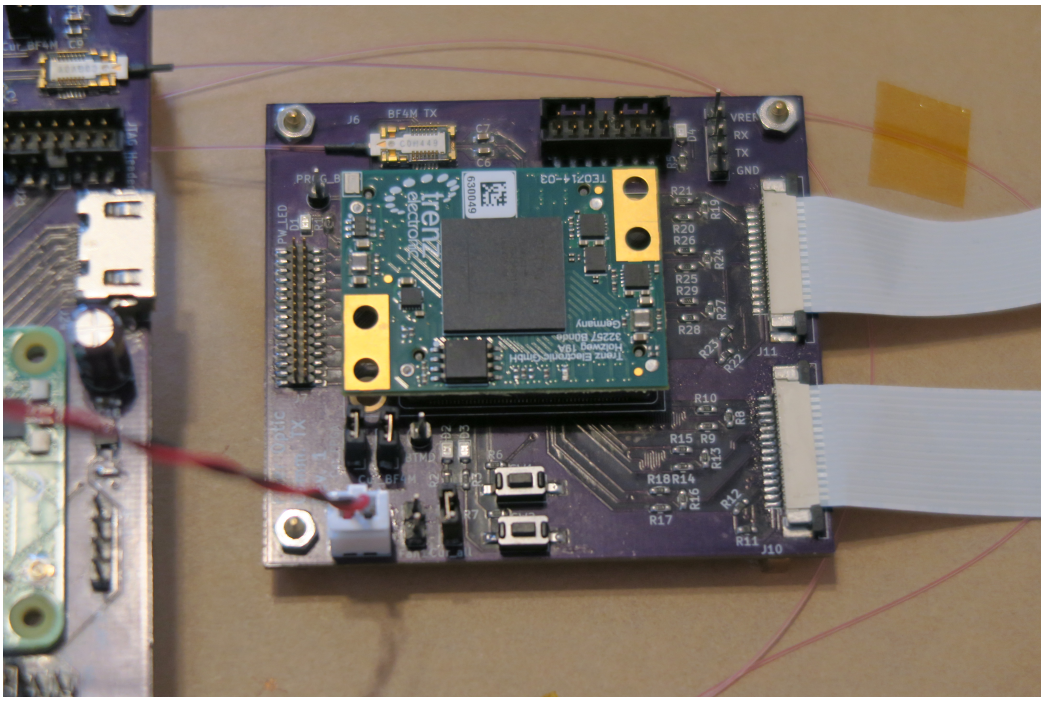

Figure 2.18: Image of the TX board

transferring the images to /dev/null at 30 fps, storing the data to RAM resulted in data loss. Hardware limitation in the Raspberry Pi CM4 or Linux OS bottlenecks exist preventing the

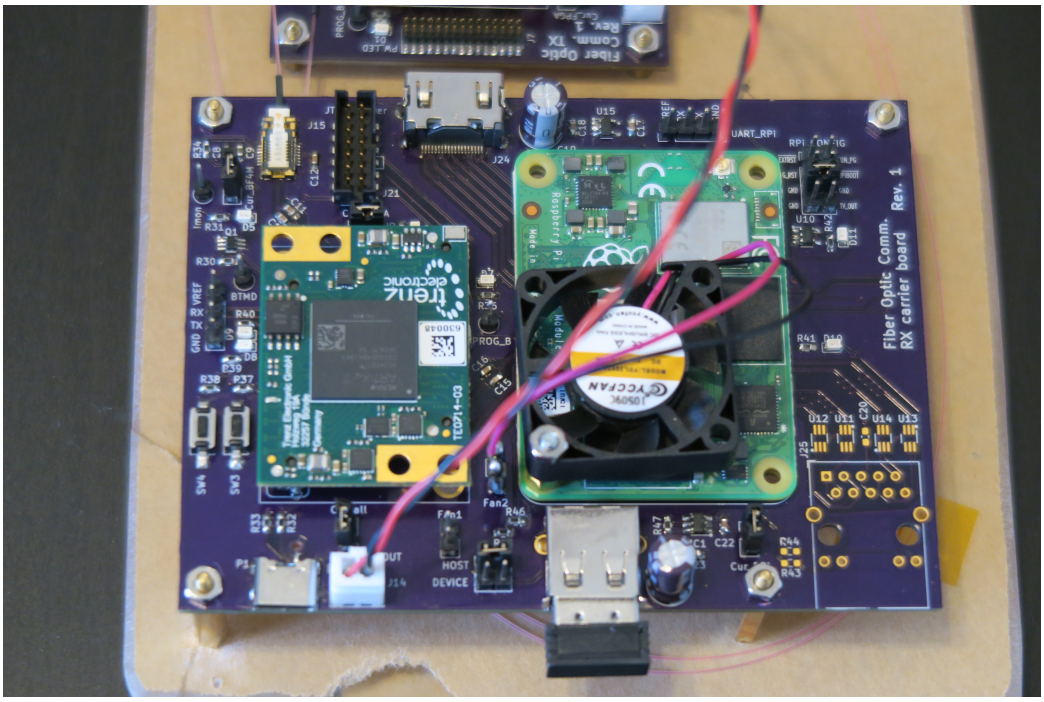

Figure 2.19: Image of the RX board

data transfer from PCIe to RAM at 30 fps as shown in the video.

CHAPTER 3

STUDIES ON FIBER-OPTIC AND OTHER DATA TRANSFER METHODS

3.1 Preliminary Studies on Environmental Testing

Table 3.1 summarizes the preliminary studies on various testing on fiber-optic transceivers in the space environment. The checkmarks indicate that the author performed the corresponding testing.

Table 3.1: Types of testing on fiber-optic performed by researchers

Author	Radiation	Thermal Cycling	Accelerated Aging	Vibration	Vacuum
Cao	✓				
Logan	✓	✓	✓	✓	
Karppinen	✓	✓		✓	✓
Heikkinen		✓		✓	

The results from the above research show that with appropriate design and manufacturing, fiber-optic modules can tolerate the harsh space environment. The following sections discuss the testing results of the fiber-optic transceivers exposed to radiation induction, various thermal conditions, thermal cycling, accelerated aging, vibration, and a vacuum environment.

3.1.1 Radiation

Optical fibers are sensitive to gamma radiation, and it mainly attenuates the optical level in the fiber[2]. NASA also considers the total ionizing dose as an environmental parameter to assess the reliability of fiber-optic cables in ISS[3]. Thus, the radiation-induced attenuation is a significant factor in determining the radiation effects on fiber-optic cables, and the authors listed in Table 3.1 focus on the attenuation induced by the radiation on the fiber.

Cao introduces the research results on radiation effects for optical fiber links operating

at 4.0 Gbps or higher. It is known that space radiation effects on fiber are attenuation mainly from total ionizing dose[4]. Figure 3.1 shows the attenuation with irradiation dose rate for 0.1 rad/min for SMF-28 fiber from Corning Corporation and R1310-HTA fiber from Nufern. Considering the fiber length barely exceeds 100 meters for satellite systems, the total attenuation induced by 100 krad total ionizing dose is less than 1dB. Notice that $100\,[\text{krad}]\,/0.1\,[\text{rad/min}]\,/60\,[\text{min/hour}]\,/24\,[\text{hour/day}]\,/365\,[\text{day/year}] \approx 1.9\,[\text{year}]$. Thus, the attenuation of the fiber-optic cable caused by the low dose rate will be less than 1 dB for the mission life of approximately 2 years or less.

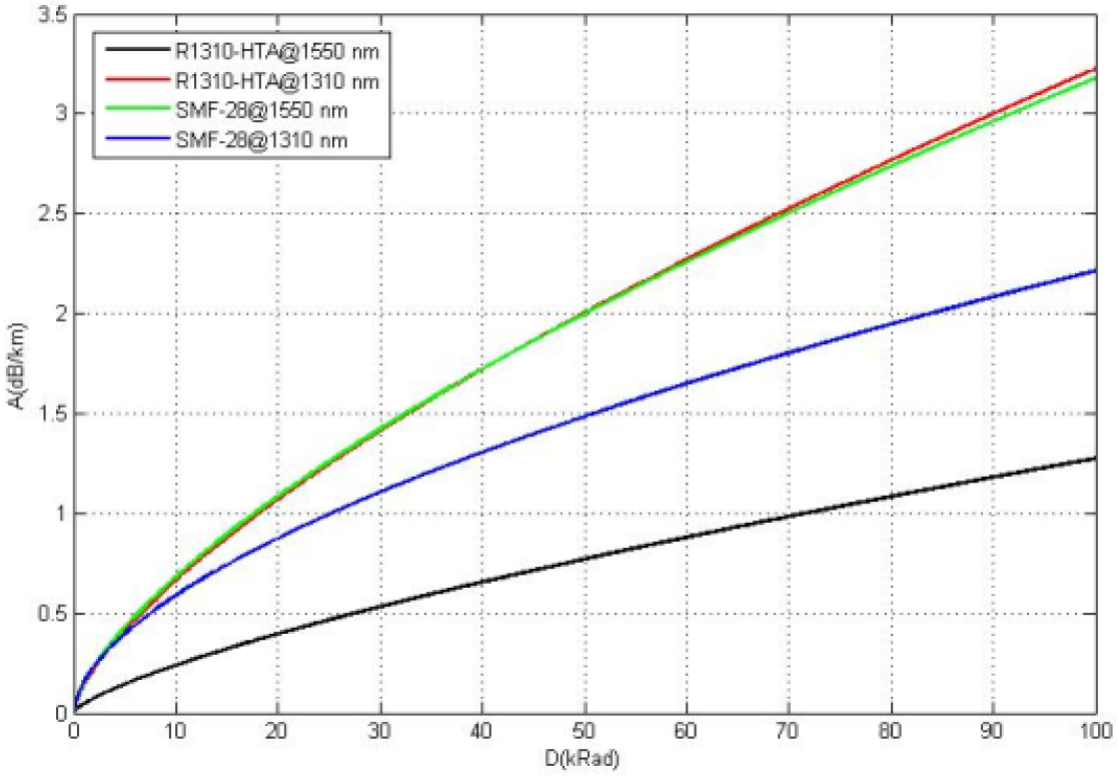

Figure 3.1: Optical fiber loss with irradiation dose at 0.1 rad/min[4]

Cao reports the radiation effects on internal chips in the optical transceiver and claims that micro-controller unit (MCU) in the optical transceivers are extremely sensitive to single event effects (SEE). Figure 3.2 and Figure 3.3 show the SEE experiment on MCU, and driver and amplifier ICs, respectively. The figures indicate that driver and amplifier ICs are relatively stronger during the SEE test, and Cao concludes that the MCU in the fiber-

optic transceiver is the most sensitive part of the fiber-optic data link system. Cao suggests using radiation-tolerant MCU in the fiber-optic transceivers to design a radiation-tolerant fiber-optic link system.

model/ company	particle	LET (MeV.c m2/mg)	Results		
			SEU	SEFI	SEL
MSP430F249(TI)	F	3.84	0	0	0
	Cl	12.6			2
	Ge	37.3			2
MSP430F2618(TI)	F	3.84	0	0	0
	Cl	12.6			2
	Ge	37.3			2
MC9S08QG8 (Freescale)	F	3.84	0	0	0
	Cl	12.6			2
	Ge	37.3			2
ADUC7023 (AD)	F	3.84	0	0	0
	Cl	12.6			2
	Ge	37.3			2

Figure 3.2: SEE experiment on MCU[4]

model/ company	particle	LET (MeV.c m^2/mg)	Results		
			SEU	SEFI	SEL
MAX15059	Cl	12.6	√	0	0
	Ge	37.3	√	0	0
GN7355	Cl	12.6	√	0	0
	Ge	37.3	√	0	0
GN2017	Cl	12.6	√	0	0
	Ge	37.3	√	0	0
GN1158	Cl	12.6	√	0	0
	Ge	37.3	√	1	0
IPVD12X12	Cl	12.6	√	0	0
	Au	85.6	√	0	0
GN1157	Cl	12.6	0	0	0
	Ge	37.3	0	0	0
	Au	85.6	0	0	0
GN2014 GN2003S	Cl	12.6	√	0	0
	Ge	37.3	0	0	0
	Au	85.6	√	0	0

Figure 3.3: SEE experiment on driver and amplifier ICs[4]

Logan conducted radiation exposure on Size #8 opto-electronic contact as shown in Figure 3.4[5]. Though the form factor was different, the functionality of converting optical to electronic and vice versa was the same as the BF4M module.

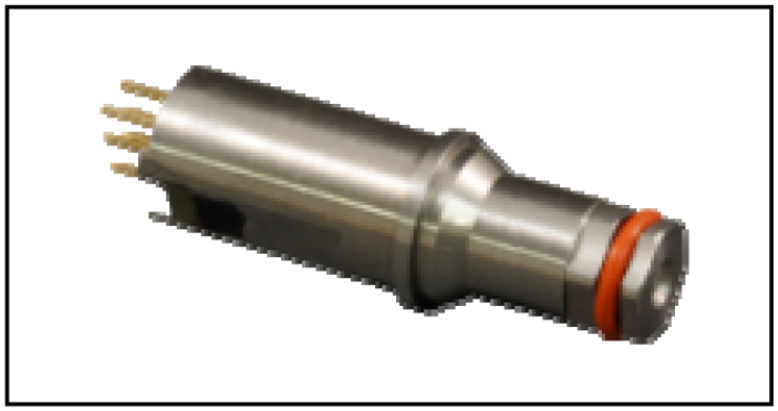

Figure 3.4: Size #8 opto-electronic contact[5]

The Size 8 contacts were exposed to the radiation of 165 krad of gamma radiation from a cobalt-60 source with 2.5×10^{12} neutrons/cm^2 while operating at 5.0 Gbps under continuous error monitoring. No errors were detected in the test[5].

Karppinen also conducted the total ionizing dose tests on the SolidOpto SPFI fiber-optic transceiver shown in Figure 3.5 with gamma radiation up to 100 krad at the rate of 541 rad/h and found no notable degradation of the performance[6].

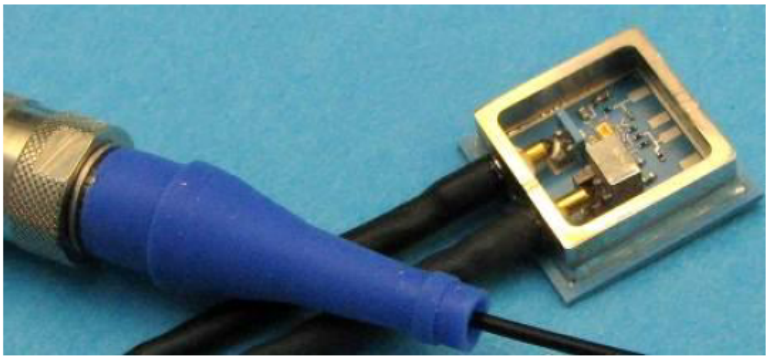

Figure 3.5: SolidOpto SPFI transceiver without sealing metal lid[6]

Karppinen further conducted heavy-ion and proton radiation tests to evaluate the SEE on the transceiver. The heavy-ion test revealed the transceiver was latch-up free at a linear energy transfer (LET) of 88.4 MeV cm^2/mg and a fluence of 20 x 10^6 cm^{-2}. The transceiver was also considered proton radiation insensitive as the maximum proton energy of 200 MeV with a fluence of 20 x 10^{10} cm^{-2} did not induce any single event transient (SET) to

the transceiver[6].

All literature studies discussed above agree that space-grade fiber-optic transceivers are available in the market and tolerable under gamma radiation. Cao suggests that the attenuation of the fiber-optic cable is less than 1 dB for a 2-year mission, so the radiation-induced attenuation of the fiber-optic cable will not be an issue for short-period missions. Additional radiation testings may be needed for a long-period mission or a deep-space mission as the radiation dose rate may differ from LEO. Cao also reports that the most sensitive part to the radiation is the MCU in fiber-optic transceivers. Hence, metal shielding as seen in Figure 3.4 and Figure 3.5 may help reduce SEE on the MCU in the BF4M module.

3.1.2 Operating Temperature

Figure 3.6 shows the eye diagram of the BF4M receiver at the temperature of -10 C° and +60 C°[7].

From the testing result, the BF4M module can safely operate in the thermal range of -10 C° and +60 C°.

3.1.3 Thermal Cycling

Logan performed a thermal cycling testing for 1000 cycles from -55 C° to +125 C° non-operating on the Size #8 contacts[5]. The contacts passed the full production tests over temperature from -40 C° to +85 C° at each interval.

Karppinen also confirmed that their SolidOpto SPFI fiber-optic transceivers achieved over 1000 cycles of temperature cycling from -55 C° to +125 C°[6].

Heikkinen carried out 80 cycles of thermal cycling from -40 C° to +85 C° on their fiber-optic transceiver during the operation, and no error was detected during the test[2].

The fiber-optic modules Logan, Karppinen, and Heikkinen used passed the thermal cycling tests. This fact supports that the fiber-optic module can tolerate the harsh thermal

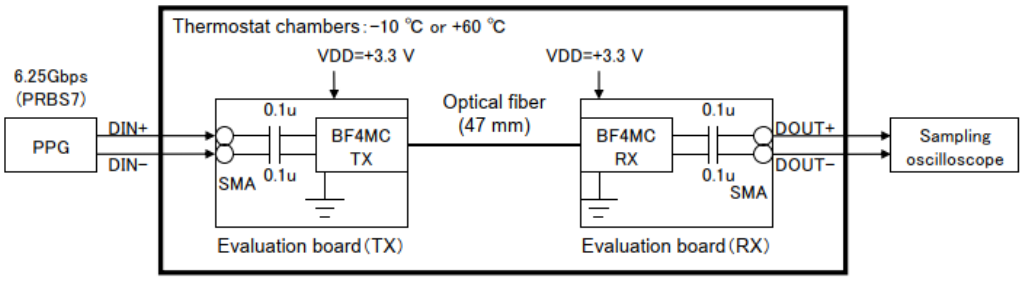

Measurement connection diagram for temperature characteristics

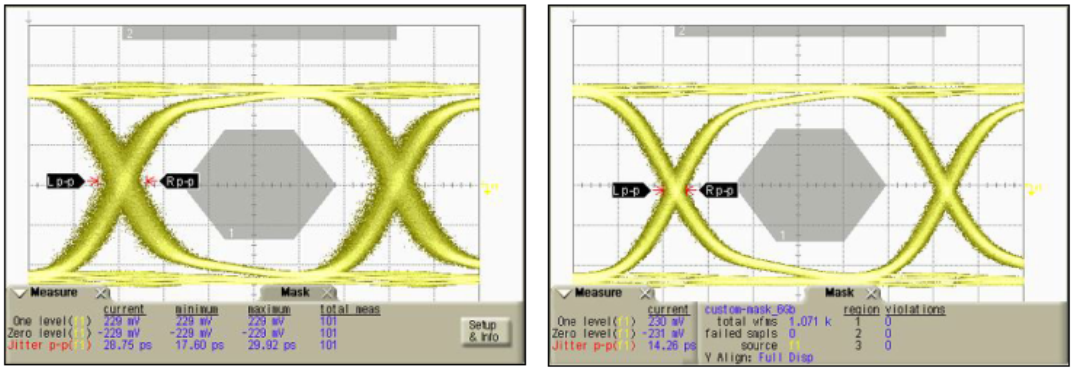

Eye diagram at -10°C **Eye diagram at +60°C**

Figure 3.6: Eye diagram of BF4M at -10 C° and +60 C°[7]

cycling in the space environment with proper design and manufacturing.

3.1.4 Accelerated Aging

Logan performed accelerated aging tests on 20 transmitters and receivers, and over 2000 hours of testing, no failure was observed. Figure 3.7 shows the transmitter output power in the top and the receiver sensitivity at 1.25 Gbps in the bottom. No degradation of the performance was observed[5].

This testing result verifies that the fiber-optic transceivers will not wear out in a short period.

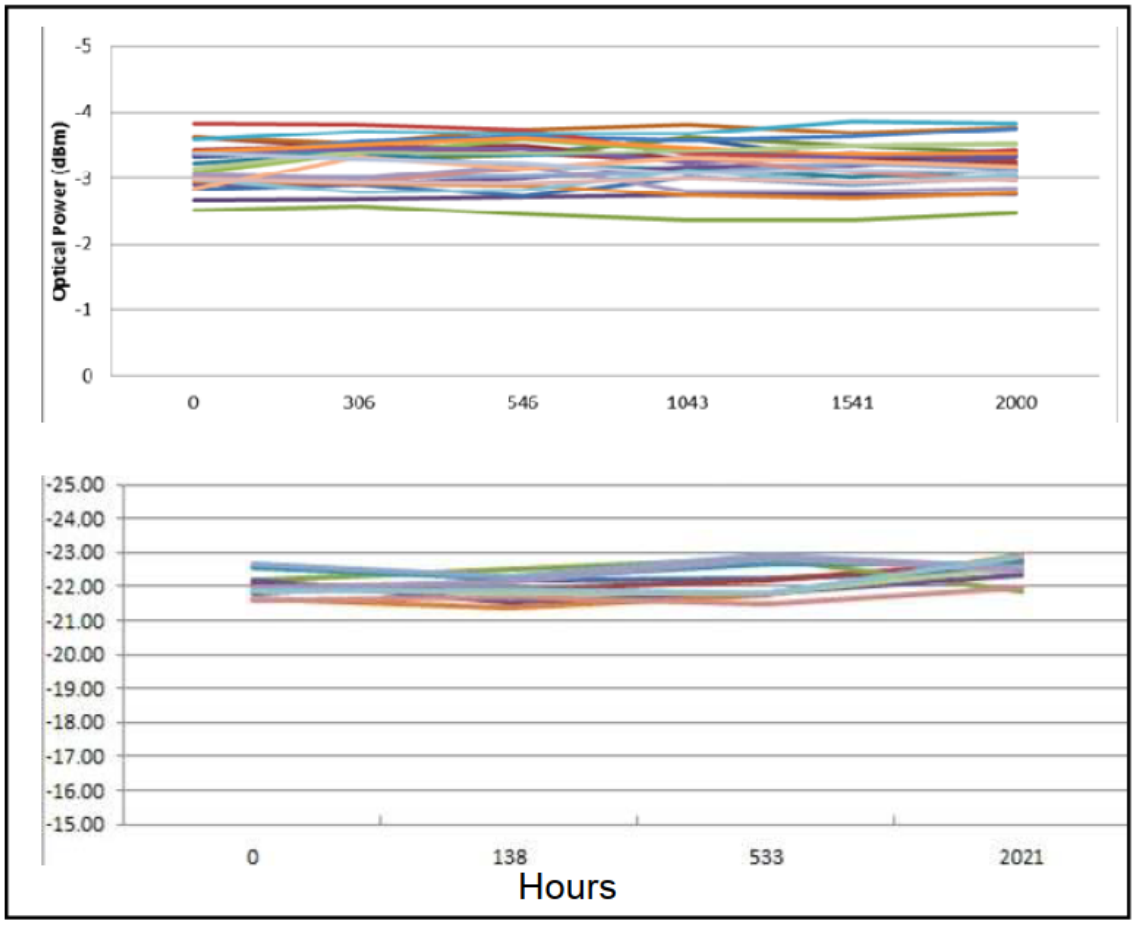

Figure 3.7: Accelerated Aging of Size #8 contacts. Transmitter output power (top) and receiver sensitivity at 1.25 Gbps (bottom)[5]

3.1.5 Vibration

Logan conducted a vibration testing to a level of 54 g_{rms} for 2 hours per axis as well as 10 0.9 ms shock pulses of 650 G per direction in all three axes while the optical link was operating at 5.0 Gbps. No error was detected during any vibration and shock tests[5].

Karppinen reports that the SolidOpto SPFI passed the mechanical vibrations and shock tests without failure. The testing included half-sine wave shock of up to 3000 g acceleration at 10 kHz and the random vibration test up to 50 g_{rms} in 3 axes [6].

Heikkinen carried out a sinusoidal vibration test from 5 to 150 Hz with a maximum acceleration of 20 g and a 10-min period of random vibration from 20 to 2000 Hz with a total level of 15.7 g_{rms} in all three axes on their fiber-optic modules. No performance

degradation was observed after the vibration tests[2].

These results from Logan, Karppinen, and Heikkinen confirm that the fiber-optic modules tolerate multiple vibration profiles with proper reinforcements of contacts.

3.1.6 Vacuum

Karppinen conducted a vacuum test on the SolidOpto SPFI transceivers and confirmed the hermeticity of the package.

This result suggests that fiber-optic transceivers can pass vacuum testing with proper material and manufacturing.

3.1.7 Summary

The above discussions of literature studies by Cao, Logan, Karppinen, and Heikkinen suggest fiber-optic transceivers can pass the space environment tests with proper design, material, and manufacturing. However, it is noted that the above studies do not validate that the BF4M fiber-optic used in this research satisfies the standards for space missions. Further radiation, thermal, mechanical, and vacuum testing are needed for the BF4M fiber-optic in the space environment. However, these tests are unfortunately outside the work of this research.

For future work, the prototype developed in this research can be used to conduct vibration testing on the BF4M module. Re-designing and re-manufacturing the prototype are required to place the prototype board in a vacuum chamber as the current version uses electrolytic capacitors for the power supply.

3.2 Space-Grade Fiber-Optic Modules

Below are some of the fiber-optic transceivers designed for space missions in the market.

AirBorn has a series of space-rated active fiber-optic products that convert electric signals in copper to optical signals in fiber which can directly be substituted with the BF4M[8].

AirBorn provides environmental testing results, including vibration, shock, vacuum, and radiation on the connectors and cables.

TE Connectivity has rugged fiber cable assemblies[9] and optical flex circuit cable assemblies[10] for space missions to interconnect subsystems within satellite systems.

NASA also publishes a database of radiation effects on commercial-off-the-shelf fiber-optic cables[11]. The database provides radiation test results on many commercial fiber-optic cables that spacecraft designers can refer to.

Although the BF4M fiber-optic module is not verified to tolerate the space environment, the space-grade fiber-optic modules are available in the market, as shown above. Hence, the high-speed fiber-optic communication demonstrated in this research in the space environment is technically feasible. One can substitute the space-grade fiber-optic module with the BF4M on the prototype to reduce the time and efforts to verify the environmental tests on the BF4M.

3.3 Comparison of Data Transfer Methods

3.3.1 Bandwidth

The BF4M can operate at up to 6.25 Gbps as implemented in this prototype. Although 10 Gbps ethernet is available in the market today, widely-available embedded systems and single-board computers such as Raspberry Pi integrates 1.0 Gbps ethernet. It is illogical to discuss the maximum bandwidth of coax and flat flex cables as they are the types of conductors, and their bandwidth is determined by the signal standard and how they are implemented. However, for the Artix-7 series, 6.25 Gbps is the theoretical maximum bandwidth for a coax cable and one lane of FFC. Table 3.2 compares the bandwidth of each transfer method.

Table 3.2: Maximum bandwidth of BF4M, ethernet, coax, and FFC

	BF4M	Ethernet	Coax	FFC
Bandwidth	6.25 Gbps	1.0 Gbps	6.25 Gbps*	6.25 Gbps*

3.3.2 Cable Flexibility

Cable flexibility is measured by the minimum bending radius of each transfer method. As shown in Figure 3.9, the BF4M has a thin and flexible cable whose minimum bending radius is 10 mm[7]. This feature enables flexible routings within the CubeSat platform.

The ethernet and coax cable enclose copper wires and layers of shielding, contributing to the stiffness of the cables. The minimum bending radius is about 25 mm for ethernet[12] and ranges from 13 mm to 50 mm for a coax cable[13].

The flexibility of FFC is similar to that of the fiber-optic cable on one axis, but FFC must be bent to go perpendicular to the wires running parallel to each other. ES&S Solutions GmbH reports that the minimum bending radius of FFC is 5 mm[14].

Table 3.3: Minimum bending radius of BF4M, ethernet, coax, and FFC

	BF4M	Ethernet	Coax	FFC
Min. Bending Radius	10 mm	25 mm	13 - 50 mm	5 mm

Although FFC is the most flexible cable in terms of the minimum bending radius, it is not flexible in every direction as FFC has multiple conductors running parallel to each other. The BF4M's minimum bending radius is twice that of the FFC, but it does not have a constraint on the direction of the cable.

3.3.3 Power Consumption

This section discusses the power consumption of each data transfer method's physical layer. As baseline ethernet ICs to be compared with the BF4M module, two ethernet PHY ICs from Texas Instruments are chosen: Space-grade DP83561-SP and low-power DP83867. From the datasheets, the typical power consumption of DP83561-SP operating at 1.0 Gbps is 855 mW[15], DP83867 operating at 1.0 Gbps is 454 mW[16], and the maximum power consumption of the BF4M operating at 6.25 Gbps is 22.4 mW for a TX module and 64.4 mW for a RX module as shown in Subsection 2.4.2.

Since coax and FFC are passive cables and do not require additional components to transfer data, the power consumptions of these cables are negligibly minor in the context of this research.

Since each system needs TX and RX components, one for a transceiver and the other for a receiver, the power consumptions of a pair of the ethernet PHY ICs and the BF4M module are used for the comparison. Table 3.4 shows the power consumptions of the pairs of the ethernet PHY ICs and the BF4M.

Table 3.4: Power consumptions of the ethernet PHY ICs, the BF4M transceiver, Coax, and FFC

	BF4M	DP83561-SP	DP83867	Coax	FFC
Power Consumption	90 mW	1710 mW	908 mW	≈ 0 W	≈ 0 W

The BF4M module signifies its low power consumption compared to the ethernet PHY ICs. Even though this power consumption is a drawback compared to coax or FFC, it is a small value that would not be problematic unless the design requires a tight power budget.

3.3.4 Transmission Length

Considering -3 dB is the threshold for the maximum transmission length, the maximum transmission length of the low-loss coax cable is 10 m, and SpaceFiber coax is 1 m, as shown in Figure 3.8[17]. SpaceFiber is standardized fiber-optic transmission by ESA to enable high data-rate data handling, including synthetic aperture radar and multi-spectral imaging systems.

The theoretical maximum transmission length of ethernet is 100 m. The maximum transmission length of FFC cannot be determined as it solely depends on the signal speed, level, and design, but it is safe to assume the maximum transmission length for FFC is less than approximately 50 cm as FFC does not come with a layer of shielding.

Table 3.5 compares the maximum transmission length of each method.

Table 3.5 reveals that for the long-distance data transfer, the fiber-optic communication

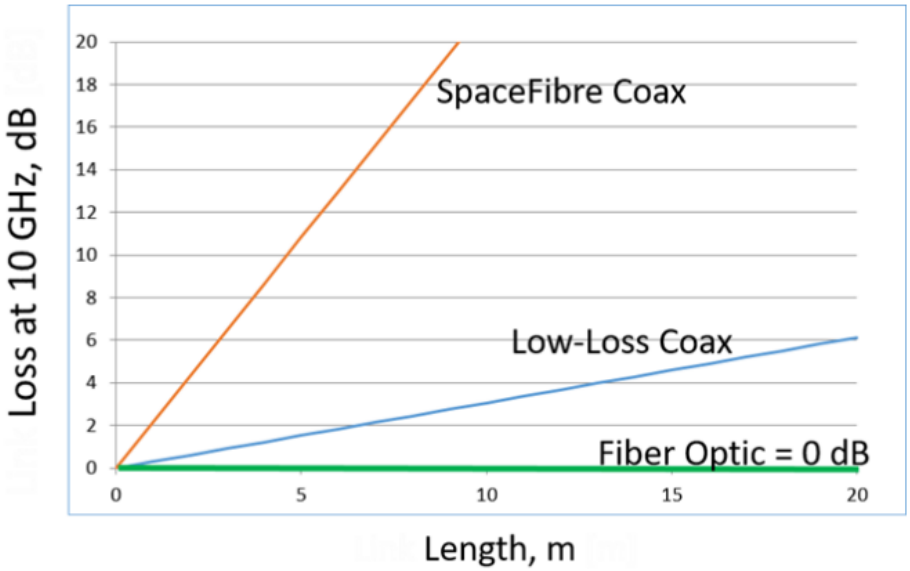

Figure 3.8: Loss in dB at 10 GHz for SpaceFibre coax, low-loss coax, and fiber-optic link[17]

Table 3.5: Maximum transmission length of each transfer method

	BF4M	Ethernet	SpaceFiber coax	Low-loss coax	FFC
Max. Trans. Len.	>100 m	<100 m	<1 m	<10 m	<50 cm

enabling the data transfer of over 100 m is the suitable solution among these methods.

3.3.5 Cable Weight

Table 3.6 summaries the cable weight per meter for gigabit ethernet[18], SpaceFibre coax, and a loss-less coax[5]. The weight of a 1 m BF4M and a 20 cm 15 conductor FFC is measured with a scale.

Table 3.6: Cable weight per meter

	BF4M	Ethernet	SpaceFiber	Loss-Less Coax	FFC
Cable Mass	0.50 g/m	49 g/m	48 g/m	223 g/m	5.6 g/m

Table 3.6 shows that the weight of the BF4M is significantly less than that of ethernet and a coax cable; thus, the BF4M can contribute to the reduction of mass in the CubeSat platform.

3.3.6 Connector Size

Figure 3.9 shows the dimensions of the BF4M cable and plugs. The plug is in a small footprint, and the diameter of the cable is 0.5 mm. These characteristics are suitable in CubeSat platforms with strict constraints on volume and provide flexibility in design.

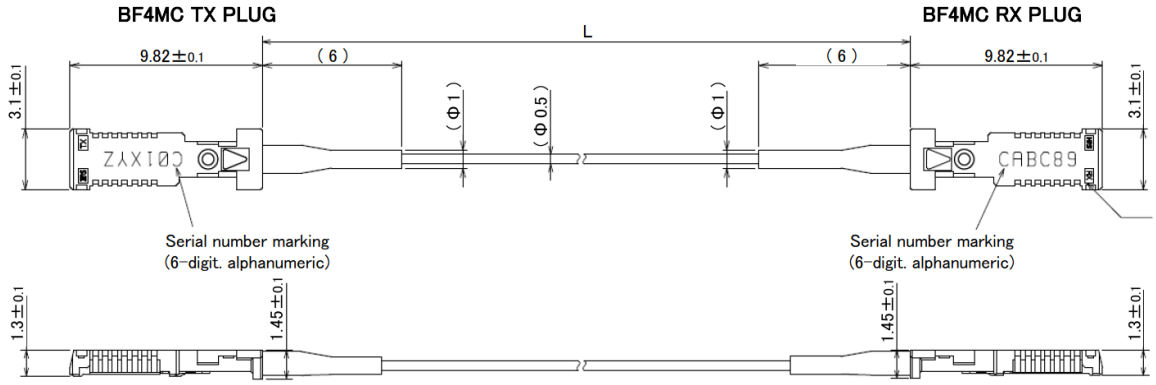

Figure 3.9: Dimension of the BF4M fiber-optic module[7]

The size of the BF4M receptacles is 5 mm x 10 mm, and their height is 1.5 mm[7]. The size of the RJ45 connector from Amphenol is 18 mm x 16 mm, and its height is 12 mm[19]. The SMA connector is the common connector for a coax cable on FPGA boards, and its size is approximately 8 mm x 10 mm, and its height is about 20 mm[20]. The FFC connector is for a 1.0 mm pitch 15 pin cable, and its size is 20 mm x 7.3 mm with a height of 2.7 mm[21]. Table 3.7 shows the volume of each connector size.

Table 3.7: Connector size in volume

	BF4M	RJ45(Ethernet)	SMA Connector	FFC connector
Connector Size	75 mm^3	3456 mm^3	1600 mm^3	394 mm^3

The compactness of the BF4M receptacle is notable, and this small factor connector provides some flexibility in the CubeSat platform.

3.3.7 Electrical Isolation and EMI

The fiber-optic communication system has electrical isolation in the same way a photocoupler isolates one circuit from another. Enhanced electrical isolation improves reliability and

reduces common-mode noise by isolating MCU from end devices such as sensors operating at high voltage.

A fiber-optic system is also immune to EMI since it is a non-conductive material. Ethernet, coax, and FFC are conductive materials; thus, they do not offer electrical isolation or EMI immunity by themselves.

3.3.8 Summary

Table 3.8 summaries the comparisons of the data transfer methods discussed above. It is noted that the bandwidth of coax and FFC are greatly affected by the design and implementation. The bandwidth of 6.25 Gbps for coax and FFC is a theoretical maximum value. The BF4M achieves high bandwidth and consumes the minimum power with a flexible fiber-optic cable and small-footprint connectors among the high-speed data transfer methods. It also can transmit signals without attenuation over a long distance.

The comparison of overall system mass and volume of each transfer method is not performed as overall hardware architecture significantly differs in each transfer method, and it is highly application dependent.

Table 3.8: Comparison of data transfer methods at a glance

	BF4M	Ethernet	Coax	FFC
Bandwidth	6.25 Gbps	1.0 Gbps	6.25 Gbps*	6.25 Gbps*
Cable Flexibility	○	×	×	△
Power Consumption	90 mW	900 - 1700 mW	≈ 0 W	≈ 0 W
Max. Trans. Len.	>100 m	<100 m	1 - 10 m	<50 cm
Cable Weight	0.50 g/m	49 g/m	48 - 223 g/m	5.6 g/m
Connector Size	75 mm^3	3456 mm^3	1600 mm^3	394 mm^3
Electrical Isolation and EMI	○	×	×	×

CHAPTER 4
DISCUSSION

4.1 Potential Application

This high-speed fiber-optic interface could be utilized in many applications. The following sections discuss the potential applications of utilizing fiber-optic communication.

4.1.1 High-Speed ADC

With advances in electronic components, sensors are becoming common to produce an unprecedented amount of data that spacecraft cannot fully handle. For example, a high-resolution camera used in this research produces 1920×1080 [pixels/frame] $\times 16$ [bits/pixel] $\times$ 30 [fps] $\times\ 2 \approx 2.0$ Gbps of raw data at 30 FPS. Before any post-processing is performed on the raw data, this data stream from the sensor must be transferred to a post-processing processor. The prototype developed in this research successfully transferred approximately 2.0 Gbps of raw data to a processor. Thus, the prototype is a demonstration of the interconnection for high-speed analog-to-digital converter (ADC). This section lists other mission examples requiring high-speed ADCs.

Stereo Imaging

Stereo imaging for proximity operations can be implemented with minor modifications to the dual-imaging display demonstration developed in this research. Stereo imaging algorithms implemented by C++ or Python can directly use the raw image data transferred from the camera modules to the Raspberry Pi CM4. The Raspberry Pi CM4 allows any user-developed application to utilize real-time raw image data.

Earth Observation

The high-speed interconnection between the sensors and the processors is necessary for earth observations using synthetic aperture radar (SAR). Sentinel-1, developed by ESA, requires an interconnect data rate of 1.28 Gbps for its synthetic aperture radar[22].

4.1.2 Interconnection within Large Structure

One of many advantages of fiber-optic transceivers is long-distance data transfer, and ISS uses a fiber-optic cable to transfer data up to 100 m[11]. Hence, a fiber-optic is suitable for interconnections within large structures.

4.1.3 Additional Design Flexibility

Fiber-optic communication allows for additional design flexibility. An example scenario is that sensors at a tip of a rover arm generate a high volume of data. A traditional way to transfer data may be post-processing the generated data within a processor placed close to the sensors to reduce the amount of data and then send the reduced data to a central processor. If fiber-optic transceivers are adopted, post-processing near the sensors is no longer needed. The raw data can be directly transferred to the central processor, which may be protected from radiation with multiple shielding layers. In this case, the overall system can be simplified by removing the post-processing component. Hence, a fiber-optic communication system offers designers additional options to achieve missions.

4.1.4 Ka-Band RF Downlink

TDRSS F10 spacecraft developed by NASA demonstrated in the field 1.5 Gbps and 2.0 Gbps Ka-Band RF communication, and up to 20 Gbps data transmission over Ka-Band frequency is achieved in a laboratory to be used as a downlink method in the future[23]. To utilize this high data rate of Ka-Band RF communication, the data rate of interconnection

must be greater than that of the Ka-Band RF communication. Here, fiber-optic communication is a suitable candidate as multiple lanes of fiber-optic can transfer 20 Gbps of data.

4.1.5 Free-Space Optical Communication

The Aerospace Corporation's AeroCube-7 is a NASA-funded project to demonstrate the feasibility of the low-earth orbit (LEO) to ground high-speed laser communication and achieved 200 Mbps free-space laser communication from LEO to ground in 2018[24]. A 10 W laser diode is used in the 1.5U CubeSat platform. Figure 4.1 shows the system overview of the downlink transmitter loaded in the 1.5U platform[25].

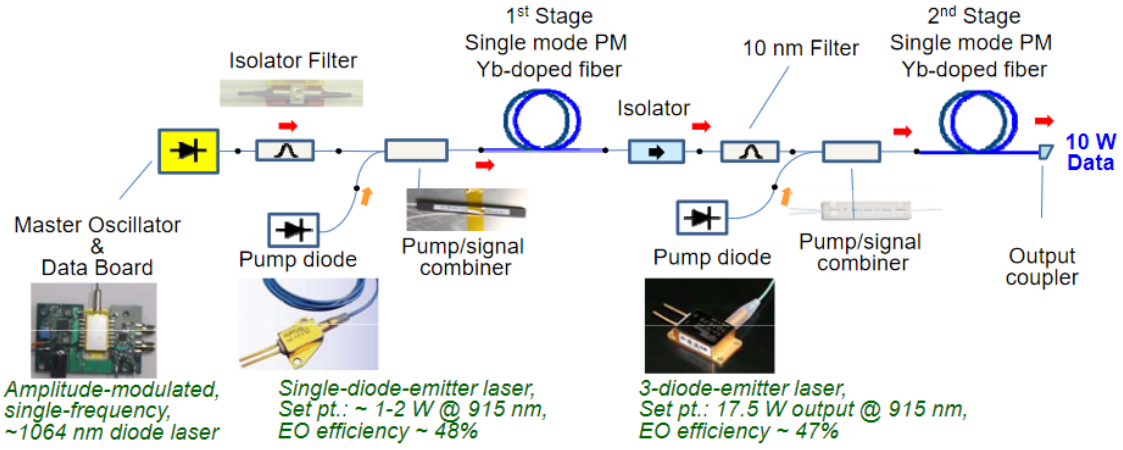

Figure 4.1: Schematic of laser downlink transmitter[25]

An optical ground station to receive and decode the free-space optical communication is also available. The Aerospace Corporation owns two optical receiving ground stations at Mt. Wilson, CA, as shown in Figure 4.2[25].

Although many challenges, such as a precise alignment mechanism, must be addressed, the Aerospace Corporation's AeroCube-7 mission demonstrated that the LEO-to-ground free-space optical link is technically feasible. The prototype developed in this research could be used by replacing the BF4M fiber-optic connectors with the transmitter system as shown in Figure 4.1 to realize a free-space optical communication.

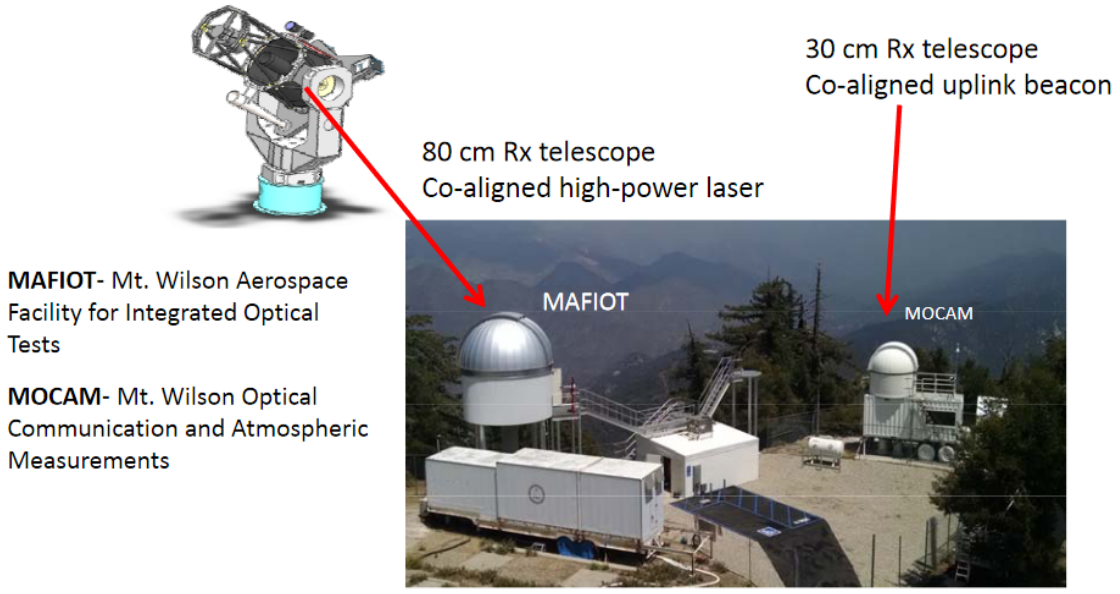

Figure 4.2: The Aerospace Corporation's optical ground stations[25]

Additionally, the foundations of the prototype can be used to achieve free-space optical communication in a formation flight. Many challenges such as transceiver and receiver alignment exist as discussed in the free-space optical communication from LEO to ground; however, the prototype in this research can contribute to the hardware design and the FPGA and post-processor implementation of the free-space optical communication in a formation flight.

4.1.6 Miscellaneous

Fiber-optic communication can be utilized in applications other than the ones discussed above. RF over fiber-optic is another technology that substitutes heavy, lossy, and EMI-prone coax cables[26]. Tethered CubeSat is another potential application. NASA proposes a potential mission of tethered CubeSat to study the surface of the Moon, in which fiber-optic may be a candidate high-speed communication system between the two CubeSats[27]. Mitsubishi Electric Research Laboratories holds a U.S. patent on tethered satellites with loose fiber-optic[28]. Moccia proposes tethered synthetic aperture radar system, in which fiber-optic communication may be a suitable interconnection between the teth-

ered satellites[29]. Hence, the application of fiber-optic communication is not limited to the ones discussed in this chapter.

4.2 Selection Guide

Although the advantages of using the fiber-optic over other traditional data transfer methods are discussed throughout this thesis, it is not the best solution for an intra-satellite communication system in all cases. The low-level hardware and software development involving hardware description language (HDL) coding and high-speed PCB designing is essential to utilize the fiber-optic data transfer. Given that the time and efforts allocated to any mission are constrained, designers should consider using traditional data transfer methods such as ethernet, coax cables, and FFC discussed above to minimize the development cost and allocate more resources to the development of mission-critical systems. Table 4.1 summaries the advantages and disadvantages of fiber-optic communication.

Table 4.1: Advantages and disadvantages of fiber-optic communication

Advantages	**Disadvantages**
• High bandwidth • Low-power consumption • Low-profile design • Flexible fiber-optic cable • Long-distance data transmission (>100m) • Improved electrical isolation • High EMI resistance	• Requires time-consuming FPGA development involving HDL coding • Involved PCB design such as impedance matching and differential signaling • More expensive than traditional methods • Space environmental tolerance is not yet verified

Some guidelines of whether using the fiber-optic as a data transfer method is appropriate, along with a few examples, are discussed below.

1. Need 1.0 Gbps or a higher data rate?

    - Candidates are fiber-optic, coax cable, and FFC.
    - If the transmission is a short distance, a coax or FFC may be preferred as no additional power is required, and they are much cheaper.

2. Data transfer over a distance of 10 m or longer?

    - Use fiber-optic to minimize the signal loss

3. Need lightweight and flexible cables for wiring within the satellite?

    - Use fiber-optic for high data rate or FFC for a cheaper option

4. Using a single board computer?

    - Unable to utilize the fiber-optic as a single board computer barely integrates high-speed low-voltage differential signal (LVDS) IOs required for interfacing with a fiber-optic module.
    - Ethernet is the typical solution for high-speed data transfer up to 1.0 Gbps on a single board computer. To achieve a higher data rate, consider using a SoC FPGA board integrating the LVDS IOs.

4.2.1 Example Cases

Below illustrate some examples of choosing the fiber-optic solution or other data transfer methods.

1. Spacecraft is equipped with multiple sensors, each generating a few hundred Mbps of data. The collected data should be post-processed in the central processor located in the middle of the spacecraft. The room in the spacecraft is limited as well.

- The fiber-optic cable is suitable for the data transfer method between the sensors and the processor as the fiber-optic can handle the high throughput data transfer for the sensors, and the flexible and thin optical cables simplify the routing between the sensors and the processor even if the room inside the spacecraft is limited.

2. Sensors generate ˜1.0 Gbps of data but can significantly reduce the data rate by post-processing the generated data. Additional processors can be placed close to the sensors for post-processing the generated data. The financial cost and development efforts must be minimized to achieve the fast development cycle and many trials.

    - FFC is suitable for the data transfer method between the sensors and the post-processing processor as FFC can handle the data rate of ˜1.0 Gbps and requires no additional hardware for the data transfer. The data transmission length can be short as the processor can be placed near the sensors. In this case, the fiber-optic as a data transmission method cannot provide many benefits to the design of the spacecraft for this mission.

4.3 Future Work

For the BF4M fiber-optic transceiver to be used in space missions, comprehensive environmental testing such as radiation, vibration, thermal, and vacuum testing must be conducted. The prototype board can be used to conduct vibration testing. Re-designing and re-manufacturing the prototype are required for vacuum testing as the current prototype uses electrolytic capacitors.

As the technical details are available at the Github repository, future designers can use the documentation and the prototype developed in this research as a reference and develop their application integrating the BF4M module.

CHAPTER 5
CONCLUSION

This research demonstrates the interconnection link of up to 6.25 Gbps with the BF4M fiber-optic module. The BF4M module also shows the low power consumption of 90 mW at 6.25 Gbps. A prototype was developed to demonstrate a dual imaging display as an example application. It utilizes two high-resolution camera modules and the BF4M fiber-optic module to transfer image data from one FPGA to another. The dual images are ultimately transferred to a Raspberry Pi Computer Module 4 via PCIe to display the images in a raw data format on a monitor. The success of this research reveals that using a lightweight, low-profile, and low-power fiber-optic module with a flexible fiber cable for subsystem interconnections allows for flexible CubeSat design and enables the high-speed data transmission of up to 6.25 Gbps. Many applications, including stereo-imaging, interconnections for high-speed ADCs and within large structures, and free-space optical communications, could be achieved with the fiber-optic communication systems.

The thesis also analyzes and compares the fiber-optic module with ethernet, coax, and FFC, current solutions to high-speed communication in CubeSat platforms. Overall, the BF4M fiber-optic module offers low signal attenuation, enhanced electrical isolation, high EMI tolerance, and a small footprint transceiver with a flexible cable, in addition to high-speed and low power consumption characteristics.

For future reference, hardware and software development details are documented and uploaded to the GitHub repository (https://github.com/kotaniko/dual-imaging). However, it is noted that environmental testing for the space environment, such as vibration, shock, and thermal cycling, needs to be performed for the BF4M module to be used in space missions.

REFERENCES

[1] C. Ciminelli, F. Dell'Olio, M. N. Armenise, F. Iacomacci, F. Pasquali, and R. Formaro, "Design and optimization of a fiber optic data link for new generation onboard SAR processing architectures," in *International Conference on Space Optics — ICSO 2012*, B. Cugny, E. Armandillo, and N. Karafolas, Eds., International Society for Optics and Photonics, vol. 10564, SPIE, 2017, pp. 371–376. [Online]. Available: https://doi.org/10.1117/12.2309038.

[2] V. Heikkinen *et al.*, "Fiber-Optic Transceiver Module for High-Speed Intrasatellite Networks," *Journal of Lightwave Technology*, vol. 25, no. 5, pp. 1213–1223, 2007. [Online]. Available: https://ieeexplore.ieee.org/document/4167956.

[3] M. N. Ott and P. R. Friedberg, "Technology validation of optical fiber cables for space flight environments," in *Optical Devices for Fiber Communication II*, D. K. Paul *et al.*, Eds., International Society for Optics and Photonics, vol. 4216, SPIE, 2001, pp. 206–217. [Online]. Available: https://doi.org/10.1117/12.414117.

[4] S. Z. Cao and Y. Zhan, "Space radiation effects on optical fiber communication links and design suggestions," *15th International Conference on Optical Communications and Networks*, pp. 1–3, 2016. [Online]. Available: https://ieeexplore.ieee.org/document/7875758.

[5] R. T. Logan, "Ruggedized photonic transceivers for spacecraft datalinks: SpaceFibre session, long paper," in *2016 International SpaceWire Conference (SpaceWire)*, 2016, pp. 1–5. [Online]. Available: https://ieeexplore.ieee.org/document/7771598.

[6] M. Karppinen *et al.*, "Radiation Tolerant Optical Transceivers for SpaceFibre Data Links," in *International SpaceWire Conference 2018*, Oulu, Finland: SpaceWire, 2018, pp. 87–91. [Online]. Available: http://2018.spacewire-conference.org/downloads/2018SpWProceedingsnew.pdf.

[7] Hirose Electric, *Hirose Active Optical Connector BF4MC Series Design Note*, Rev. 1.4, Jan. 2020. [Online]. Available: https://www.hirose.com/en/product/document?clcode=&productname=&series=BF4M&documenttype=Guideline&lang=en&documentid=D166284_en (visited on 04/23/2022).

[8] AirBorn, *AirBorn Active Optical Cable Catalog*, 2021. [Online]. Available: https://www.airborn.com/docs/openaccessprovider/catalogs/focus-aoc-catalog-web-3-21.pdf (visited on 04/23/2022).

[9] TE Connectivity. "Rugged Fiber Cable Assemblies." (2022), [Online]. Available: https://www.te.com/global-en/product-8-2061432-1.html (visited on 04/23/2022).

[10] ——, *High Density Versatile Optical Flex Circuit Cable Assemblies*, 2022. [Online]. Available: https://www.te.com/usa-en/about-te/news-center/adm-optical-flex-circuit-cable-assemblies.html (visited on 04/23/2022).

[11] M. N. Ott, "Radiation Effects Data on Commercially Available Optical Fiber: Database Summary," in *IEEE Radiation Effects Data Workshop*, 2002, pp. 24–31.

[12] NVENT, *BEND RADIUS OVERVIEW REFERENCE SHEET*, Mar. 2022. [Online]. Available: https://www.freepatentsonline.com/y2020/0313770.html (visited on 04/23/2022).

[13] PIC Wire & Cable, *Aircraft Cable Bend Radius*, Mar. 2022. [Online]. Available: https://www.picwire.com/resources/technical-articles/cable-bend-radius/ (visited on 04/23/2022).

[14] ES&S Solutions GmbH. "FFC bending test - tolerances." (2022), [Online]. Available: https://www.esskabel.de/en/product/biegezyklen-toleranzen/ (visited on 04/23/2022).

[15] Texas Instruments, *DP83561-SP Radiation-Hardness-Assured (RHA), 10/100/1000 Ethernet PHY Transceiver with SEFI Handling Sub-System*, Jun. 2021. [Online]. Available: https://www.ti.com/lit/ds/symlink/dp83561-sp.pdf (visited on 04/23/2022).

[16] ——, *DP83867E/IS/CS/IR/CR RGZ Power Consumption Data*, Oct. 2015. [Online]. Available: https://www.ti.com/lit/an/snla241/snla241.pdf (visited on 04/23/2022).

[17] R. T. L. Jr. and D. Basuita, "Mass-reduction of high-speed spacecraft datalinks enabled by rugged photonic transceivers," in *International Conference on Space Optics — ICSO 2018*, Z. Sodnik, N. Karafolas, and B. Cugny, Eds., International Society for Optics and Photonics, vol. 11180, SPIE, 2019, pp. 1618–1628. [Online]. Available: https://doi.org/10.1117/12.2536076.

[18] PIC Wire & Cable, *PIC DataMates Ethernet*, Mar. 2022. [Online]. Available: https://www.picwire.com/wp-content/uploads/files/pdfs/overviews/PIC_HSD_Product_Line.pdf (visited on 04/23/2022).

[19] Amphenol. "RJ45 Connector." (2012), [Online]. Available: https://cdn.amphenol-cs.com/media/wysiwyg/files/drawing/rje7318800xxx0x.pdf (visited on 04/23/2022).

[20] TE Connectivity. "SMA Connector." (2020), [Online]. Available: https://www.mouser.com/datasheet/2/418/8/ENG_CD_2081875_A-2324466.pdf (visited on 04/23/2022).

[21] Amphenol. "FFC Connector." (2009), [Online]. Available: https://cdn.amphenol-icc.com/media/wysiwyg/files/drawing/sfw12lf.pdf (visited on 04/23/2022).

[22] ESA. "Copernicus: Sentinel-1 — The SAR Imaging Constellation for Land and Ocean Services." (2022), [Online]. Available: https://eoportal.org/web/eoportal/satellite-missions/c-missions/copernicus-sentinel-1 (visited on 04/23/2022).

[23] FLC. "Demonstration of Multi-Gigabit Per Second Data Rates Through Ka-Band Frequencies." (2011), [Online]. Available: https://federallabs.org/news/demonstration-of-multi-gigabit-per-second-data-rates-through-ka-band-frequencies (visited on 04/23/2022).

[24] Aerospace Corporation, *Aerospace's Aerocube Program*, Aug. 2021. [Online]. Available: https://aerospace.org/sites/default/files/2021-08/2021-00486_AEROSPACE_AEROCUBE_PROGRAM.pdf (visited on 04/23/2022).

[25] R. P. Welle, S. Janson, D. Rowen, and T. Rose, "Cubesat-Scale Laser Communications," Colorado, USA, 2015. [Online]. Available: https://www.spacesymposium.org/wp-content/uploads/2017/10/R.Welle_31st_Space_Symposium_Tech_Track_paper.pdf (visited on 04/23/2022).

[26] Via Lite. "What is RF over fiber technology and what are the benefits?" (2022), [Online]. Available: https://www.vialite.com/resources/guides/what-is-rf-over-fiber-technology/ (visited on 04/23/2022).

[27] NASA. "NASA Studies Tethered CubeSat Mission to Study Lunar Swirls." (Aug. 2017), [Online]. Available: https://www.nasa.gov/feature/goddard/2017/nasa-studies-tethered-cubesat-mission-to-study-lunar-swirls (visited on 04/23/2022).

[28] P. Kieran, W. Avishai, O. Philip, and D. C. Stefano, "Loose Optical Fiber Tethering Of Multiple Satellites," 20 200 313 770, Oct. 2020. [Online]. Available: https://www.freepatentsonline.com/y2020/0313770.html (visited on 04/23/2022).

[29] A. Moccia and S. Vetrella, "A tethered interferometric synthetic aperture radar (SAR) for a topographic mission," *IEEE Transactions on Geoscience and Remote Sensing*, vol. 30, no. 1, pp. 103–109, 1992. [Online]. Available: https://ieeexplore.ieee.org/document/124220 (visited on 04/23/2022).